MNRAS **000**, 1–8 (2018) Preprint 19 July 2018 Compiled using MNRAS LATEX style file v3.0

Constraining the metallicities, ages, and ionizing continua of massive star populations

J. Chisholm[1⋆], J.R. Rigby[2], M. Bayliss[3] more?
[1] *Observatoire de Genéve, Université de Genéve, 51 Ch. des Maillettes, 1290 Versoix, Switzerland*
[2] *Observational Cosmology Lab, NASA Goddard Space Flight Center, 8800 Greenbelt Rd., Greenbelt, MD 20771, USA*
[3] *MIT Kavli Institute for Astrophysics and Space Research, 77 Massachusetts Ave., Cambridge, MA 02139, USA*

19 July 2018

ABSTRACT

Key words:

1 INTRODUCTION

Throughout this paper we assume that solar metallicities of the stellar continuum is 0.02 (Leitherer et al. 1999) and that solar gas-phase metallicities are 12+log(O/H) = 8.69 (Asplund et al. 2009).

2 DATA

2.1 High-redshift observations

2.1.1 *MEGaSaURA data*

Here we predominately use spectra of eighteen star-forming galaxies from project MEGaSaURA: The Magellan Evolution of Galaxies Spectroscopic and Ultraviolet Reference Atlas (Rigby et al. 2018a) that have moderate resolution spectra taken with the Magellan Echellette (MagE) Spectrograph (Marshall et al. 2008) on the Magellan telescopes. Fourteen of these galaxies were included in the original MEGaSaURA data release (Rigby et al. 2018a), and we include four recently acquired galaxies: the Planck Arc (Rivera-Thorsen et al. 2017), SPT 03010, SPZ 0441, and SPT 2325 **need more description here**.

The data reduction techniques are described in detail in (Rigby et al. 2018a). The galaxies span a redshift range $1.6 < z < 3.5$, leading to spectral coverage of 1240–1950Å in the restframe for all eighteen galaxies, with a median resolution of $R = 3300$ (90 km s^{-1} ; 0.5 Å at 1500Å) and signal-to-noise ratio of $SNR = 21$ (Rigby et al. 2018a). We normalize the spectra to the median of the flux between 1267–1276Å in the restframe. These spectra are ideal to probe the wealth of massive star features in the ultraviolet because they have the signal-to-noise and resolution required to determine the features of galaxies on an individual basis (see Section 5). Due to the superior combination of wavelength coverage and sensitivity, the MEGaSaURA sample is the main sample that we use in this paper.

2.1.2 *High-redshift stacked data*

While the individual MEGaSaURA spectra have high signal-to-noise ratios, many of the important stellar features are very weak. By averaging many low signal-to-noise ratio observations together (often called ''stacking'', the signal-to-noise ratio increases by a factor of $\sqrt{N}$. Consequently, the composite provides an average spectrum of the ensemble of galaxies at an extremely high signal-to-noise ratio.

This stacking procedure has successfully demonstrated the average ultraviolet spectrum of galaxies at moderate redshifts (Shapley et al. 2003; Jones et al. 2012; Steidel et al. 2016; Rigby et al. 2018b; Steidel et al. 2018). We utilize this extreme boost in signal-to-noise by using two recent stacks of (1) the MEGaSaURA lensed galaxies (Rigby et al. 2018b) and (2) a stack of 30 star-forming galaxies at $z \sim 2.4$ from Steidel et al. (2016). The MEGaSaURA stack has a peak signal-to-noise ratio of 104 with an average resolution of R= 3300 of the restframe wavelength range of 900–3000Å. Similarly, the Steidel et al. (2016) stack has a peak signal-to-ratio of 38 at resolutions of R = 1400 at restframe wavelengths of 1000–2200Å.

2.2 COS observations

To increase the statistics of the fitting procedure, we increase the sample size by including 40 local star-forming galaxies at $0.00069 < z < 0.1816$ from Chisholm et al. (2016) with Hubble Space Telescope (HST) Cosmic Origins Spectrograph (COS; Green et al. 2012). The spectra are processed following the procedures in Wakker et al. (2015), and binned by 10 (30) for galaxies with signal-to-noise ratios greater (less) than 5 per pixel. These low-redshift galaxies are predominately observed with the G130M grating on COS and have spectral resolutions of R $= 10,000 - 20,000$ (measured from the Milky Way absorption lines; Chisholm et al. 2015) over the restricted restframe of 1150-1450Å. We normalize the spectra in the same wavelength regime near 1270Å as the MEGaSaURA observations. This wavelength regime restricts the spectral diagnostics of the stellar continua, consequently we pre-

⋆ Contact email: John.Chisholm@unige.ch

dominately only use these spectra to extend the sample statistics of the metallicity relations in Section 6.2.

3 STELLAR CONTINUA FITTING

3.1 Fitting procedure

We fit the stellar continua of the MEGaSaURA galaxies by assuming that the observed spectra are linear combinations of multiple bursts of single-aged stellar populations. The light from these stellar populations then propagates through ambient interstellar medium that attenuates the stellar continuum to produce the observed shape. We fit this with a uniform dust screen model as:

$$F_{\rm obs}(\lambda) = 10^{-0.4{\rm E(B\text{-}V})k(\lambda)}\Sigma_i X_i M_i(\lambda), \quad (1)$$

where E(B-V) is the stellar attenuation parameter, $k(\lambda)$ is the reddening curve from Calzetti et al. (2000), and X_i is the coefficient multiplied by the ith single-aged stellar population model, M_i. Each M_i corresponds to an instantaneous age and stellar metallicity (Z_s). Along with E(B-V), these three parameters completely describe the shape and features of the observed stellar continuum.

We mask out $\pm$500 km s^{-1} around strong ISM absorption and emission lines as well as intervening absorption lines (Rigby et al. in preparation). Further, we also manually mask out defects or other spurious features over the restframe wavelength range of 1240–2000Å. We then fit for the X_i of each model age and metallicity as well as the E(B-V) values in Equation 1 using MPFIT (Markwardt 2009).

Between 1200-2000Å, the stellar continuum is dominated by young and massive O-type stars. Consequently, we use stellar models with young ages corresponding to 1, 2, 3, 4, 5, 8, 10, 15, 20 and 40 Myr. At 1270 Å, a 20 Myr stellar population is nearly two orders of magnitude fainter than a 1 Myr stellar population, while older populations are fainter still (Leitherer et al. 1999; Eldridge et al. 2017). Moreover, the UV stellar continua of older stellar populations evolve more slowly with time (de Mello et al. 2000). Further, the effective temperature of these B-stars drops below 20,000 K which is the minimum effective temperature that the WM-BASIC code computes high-resolution stellar atmosphere models (Leitherer et al. 2010). We use the five Z_s models of 0.05, 0.2, 0.4, 1.0, and 2.0 $Z_\odot$ that are available from the Geneva stellar atmospheres (see Section 3.2. Combined, we fit each spectra with 50 different stellar population models and one free parameter for the dust attenuation using MPFIT.

3.2 Stellar Models

The key component to the fits of the stellar continua are the models used in the linear combination ($M_i(\lambda)$). To make this comparison we use both single stellar populations (Leitherer et al. 1999, 2010) and binary star models (Eldridge et al. 2017) to compare the effects that both populations may have on the ionizing and non-ionizing continua of the massive stars. We choose the stellar atmosphere models below because they are the most comparable to each other (Eldridge et al. 2017). For both models we use a standard Kroupa initial mass function (IMF; Kroupa 2001) with a broken power-law with a high-(low-) mass exponent of 2.3 (1.3) and a high-mass cut-off of 100 $M_\odot$. Stars more massive than 100 $M_\odot$ do not live longer than 1 Myr, and therefore do not contribute heavily to the stellar models used here. Steidel et al. (2016) demonstrated this by showing that the best-fit stellar continua model does not change drastically between a 300 $M_\odot$ or 100 $M_\odot$ cut-off (their fig. 7). In the next two sections, we discuss the two stellar atmosphere models that we use.

3.2.1 STARBURST99 *models*

We used the fully theoretical Geneva models with high-mass rates (Meynet et al. 1994) with stellar continuum metallicities of 0.05, 0.2, 0.4, 1.0, and 2.0 $Z_\odot$. The models have a spectral resolution of 0.4 Å, which nicely matches the spectral resolution of the MEGaSaURA spectra. We convolved the models with a Gaussian corresponding the spectral resolution of each individual spectra, as measured from the sky emission lines (Rigby et al. 2018a), and resampled the stellar models onto the wavelength grid of the observations. Each model was also normalized to the median of the spectra between 1276–1276Å, as done for the data.

These models are created using the WM-BASIC method and densely sample the left portion of the Hertzsprung-Russell diagram up to temperatures of 20,000 K (Leitherer et al. 2010). After these temperatures, WM-BASIC does not calculate high-resolution models (Leitherer et al. 2010). Consequently, we choose the ten stellar ages between 1–40 Myr listed in Section 3.1 which have stellar temperatures above 20,000 K (40 Myr ages). These models do not include the effects of W-R stars (Leitherer et al. 2010), which may impact the He II regions (see Section 6.1.2). We do not include the effects of extreme rotation (Leitherer et al. 2014) because we want to test the effects of binarity and rotation is not included in the BPASS models.

3.2.2 BPASS *models*

We use the Binary Population and Spectral Synthesis v2.1 that include binary evolution (BPASS; Stanway et al. 2016; Eldridge et al. 2017). BPASS models have a larger metallicity range, but, for consistency, we use the same five metallicities available from the STARBURST99 models. BPASS models use WM-BASIC method to create new O-star models with 1Å resolution for stars with temperature greater than 25,000 K (Eldridge et al. 2017). Temperatures less than this have the BASELv3.1 models which have spectral resolution of 20 Å (Westera et al. 2002; Le Borgne et al. 2003). This resolution is too low to diagnose many of the narrow B-star features of older stellar populations and cannot be used to distinguish the stellar population. Therefore, we cannot use BPASS models with ages greater than 20 Myr for any metallicity and cannot use the 15 Myr 1.0 and 2.0 $Z_\odot$ metallicity models either. This means that the BPASS models do not diagnose older stellar populations as well as the STARBURST99 models do. We return to this issue in Section 6.1.1.

3.3 The nebular continuum

Young massive stars produce large amounts of ionizing photons, creating large H II regions and producing free-free and free-bound continuum emission. The nebular continuum heavily contributes to the total continuum flux at young ages, low metallicities, and redder wavelengths. For a stellar continuum metallicity of 0.05 $Z_\odot$ and a stellar age of 1 Myr, the nebular continuum is 25% of the stellar continuum at 2000Å.

While the BPASS models have the option of including a nebular continua processed through CLOUDY, STARBURST99 models do not. Consequently, we created a nebular continuum for each

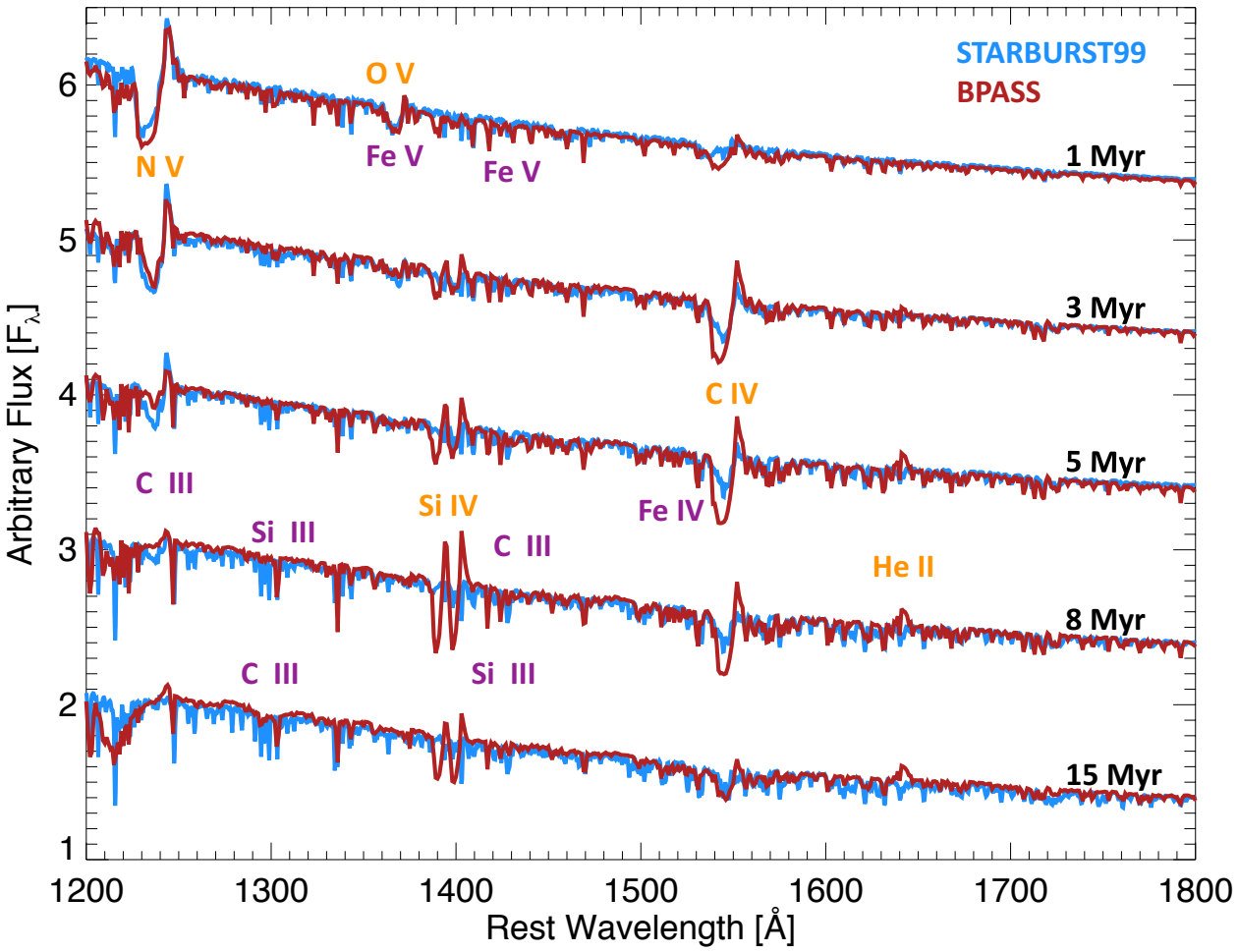

Figure 1. The fully theoretical, rest frame, single-population stellar continuum spectra of five STARBURST99 (blue) and BPASS (red) models with a metallicity of 0.2 $Z_\odot$ and decreasing age from 1 to 15 Myr (labeled on the right). Strong stellar wind (orange) and photospheric (purple) lines are labeled near the models where the features are strongest.

age, metallicity, and stellar model by processing the stellar continuum metallicity through CLOUDY. We assumed that the gas-phase metallicity and stellar metallicity were the same, a log(U) of -2.5, and $n_{\rm H} = 100$ cm^{-3}. We then added the output nebular continua to the stellar models and renormalized by the flux between 1267–1276Å. The end effect produces redder stellar models than before, and has a pronounced impact on the fitted E(B-V) of young stellar populations.

We tested the effect that different log(U) parameters have on the fitted stellar ages and metallicities by also creating models with log(U) of -2, -2.3, -2.7, and -3.0. We found that the reduced χ^2 of individual fits do not change for the different log(U) values. Consequently, we adopted a constant log(U) = -2.5 for all galaxies.

3.4 Stellar population parameters derived from the fits

From Equation 1 we derive parameters that describe the intrinsic stellar population. First, the light fraction (f_i) that each model, M_i, contributes to the total intrinsic flux at 1270Å where the models are normalized is defined as:

$$f_i = \frac{X_i}{\Sigma_i X_i}. \quad (2)$$

The light fraction measures the fraction of light that each age and metallicity contributes to the intrinsic flux. Secondly, the light-weighted age at 1270Å is defined as

$$\text{Age} = \frac{\Sigma_i X_i \text{Age}_i}{\Sigma_i X_i}. \quad (3)$$

This gives a measure of the age of the stellar population. Finally, we compute the light-weighted metallicity as:

$$Z_s = \frac{\Sigma_i X_i Z_i}{\Sigma_i X_i} \quad (4)$$

These three parameters describe the intrinsic properties of the observed stellar populations. The errors on these parameters are largely driven by the systematics of the fitting, not the statistical uncertainties. In Section 5.1.2, we compare the Z_s and Age values determined using both the BPASS and STARBURST99 models and find a 10% and 23% variation, respectively, depending on the continuum model that we used. Consequently, we quote these fractional errors for the two parameters.

Table 1. Prominent lines that distinguish between different stellar population ages. The first column gives the feature and wavelength. The second and third columns give the age range that the feature are found in a 0.4 $Z_{\odot}$ BPASS and STARBURST99 model, respectively. Metallicity also strongly impacts these features (see Fig. 3), making the detection of the individual features dependent on both age and metallicity.

Line	BPASS Age [Myr]	STARBURST99 Age [Myr]
Stellar wind lines		
N V 1240 Å	1-5	1-10
O V 1371.30	1-2	1-4
Si IV 1400 Å	3-15	3-5
C IV 1550 Å	1-15	1-10
He II 1640 Å	4-20	3-4
Photospheric lines		
C III 1247.38Å	4-15	5-40
Si III 1294.54 Å	–	5-40
C III 1290Å	–	–
Si III 1296.74 Å	–	5-40
C III 1298.93Å	–	5-40
Si II 1417.24Å	4-20	5-40
C III 1427Å	5-40	5-40
Fe V 1430.44Å	-	3-40
Fe IV 1526-1534Å	1-15	1-40
Si II 1533Å	3-10	3-40

4 RESULTS

4.1 Stellar ages and metallicities

5 WHICH SPECTRAL FEATURES DETERMINE THE STELLAR PROPERTIES?

Often times the ages of stellar populations are deduced using the broad-band SED shapes and spectral slopes. While the shape provides important age information, it is often degenerate with metallicity, and impacted by dust attenuation and nebular emission lines. By fitting the stellar spectral features with theoretical stellar templates, we simultaneously determine the age, metallicity, and dust attenuation of the stellar populations. Consequently, the light-weighted ages and metallicities discussed above are driven by spectral features of the stellar populations that are less degenerate and more robustly estimated.

The two main stellar features driving the fits are strong and broad stellar winds features and weak stellar photospheric lines. These lines can be narrow or contaminated by neighboring ISM absorption and emission features. Thus, the high signal-to-noise and moderate spectral resolutions of the MEGaSaURA and COS data are required to resolve and detect these features. In the following two subsections we discuss both spectral features individually and illustrate how the individual features determine the ages and metallicities of the stellar populations.

5.1 Stellar wind lines

The most notable stellar features in Fig. 1 are the strong and broad absorption plus emission features (orange labels; called P-Cygni profiles). The radiation fields from massive stars are strong enough to launch a stellar wind from the surface of the stars, producing the well-known P-Cygni feature (Lamers & Cassinelli 1999). The rest frame ultraviolet contains many strong, high-ionization, resonant lines that often have observed P-Cygni profiles (see Table 1).

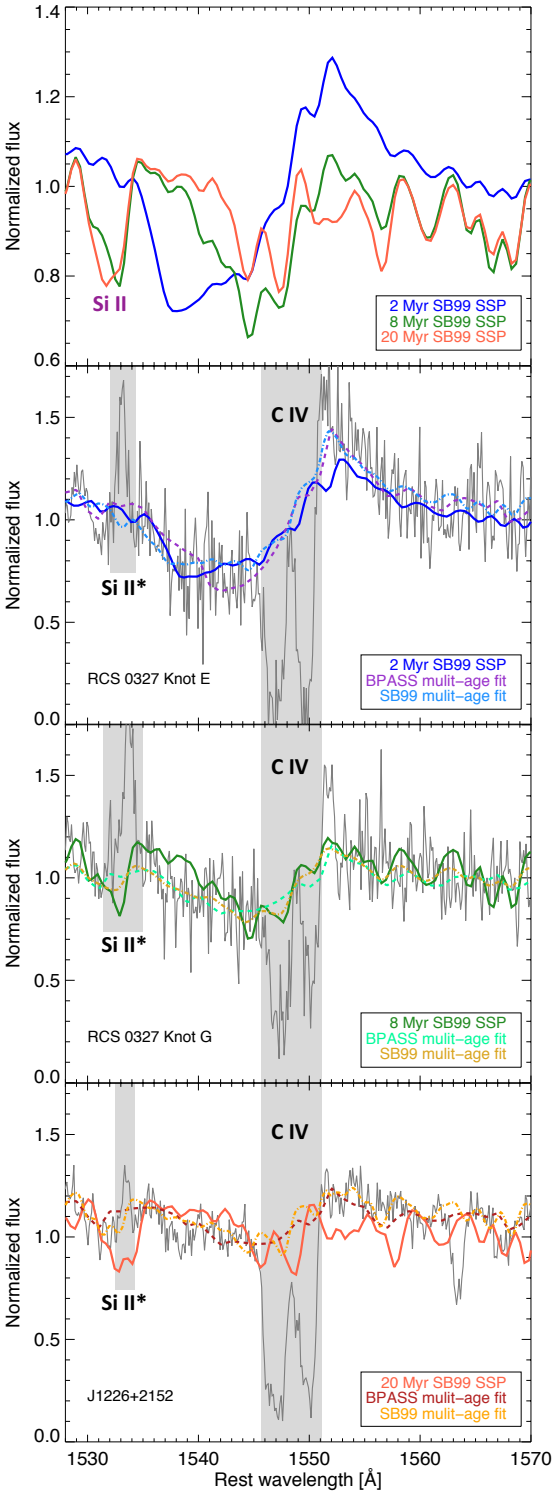

Figure 2. The variation of the C IV O-star wind region with stellar age. The top panel shows three different STARBURST99 single stellar populations (SSP) with ages of 2, 8, and 20 Myr and the same 0.2 $Z_{\odot}$ metallicity. The C IV absorption and emission dramatically decreases with increasing age. The next three panels show three galaxies (names in the lower left) with descending fitted ages of 2.6, 7.8, and 19 Myr and fitted metallicities of 0.29 ± 0.06 $Z_{\odot}$. The SSP corresponding to the fitted properties is overplotted as a solid lines. The multi-age, multi-metallicity BPASS (dashed line) and STARBURST99 (dot-dashed line) are shown in each panel. The SSPs describe the overall shape of the young C IV lines, while the multi-age fits are required to describe the full details. Gray regions indicate interstellar C IV absorption and Si II* emission.

Whether the lines are observed and the observed shapes of the P-Cygni profiles determine both the age and metallicity of the stellar population. Below we discuss the detection of these lines and how the morphologies of the P-Cygni lines help the fitting algorithm determine the stellar age and metallicity.

5.1.1 *Incidence of observed stellar wind lines*

Here we discuss the five main stellar wind lines from massive stars in the observed wavelength regime between 1200-1900Å. In general, younger populations have more highly ionized stellar winds (see the difference between N V and Si IV in Table 1 and Fig. 1 which have ionization potentials of 93 and 45 eV, respectively) because younger stars have larger temperatures, thus the presence of a particular stellar wind line provides information on the age of the stellar population. Similarly, lower metallicities mean that there are fewer metals in the stellar atmospheres, causing the wind lines to decrease in strength with metallicity (see Section 5.1.3. The incidence of stellar wind features describe both the stellar age and metallicity.

RCS-0327 Knot E, RCS-0327 Knot U, J0033+0242, and the Planck Arc (the four galaxies with the youngest fitted ages in the sample) have weak O V 1371Å wind features. O V is not observed in the rest of the sample, reinforcing the young fitted ages of these galaxies. The N V 1240Å is seen in all the galaxies, although it is weak in J1527+0652 and the Cosmic Eye (two of the oldest fitted ages). The N V profile is unique because it is fairly insensitive to metallicity and only age dependent because N V is not the dominate ionization state in typical O-star winds,N IV is the dominant ionization state. The temperature of O-stars increases with decreasing metallicity, which heats N IV gas towards the N V ionization state. This heating is nearly matched by the decrease in metallicity such that N V is nearly independent of metallicity and only an O-star indicator (Kudritzki 1998; Lamers & Cassinelli 1999). Since we detect N V in all but two of the oldest galaxies, we confirm the presence of O-stars in most of the MEGaSaURA sample.

Strong Si IV absorption is seen in most of the galaxies, but it is rarely observed as a P-Cygni feature (see the discussion in Section 3.2). P-Cygni Si IV is generally only observed in supergiants (evolved stars) because the Si IV ionization state traces cooler gas than the typical O star wind (the opposite behavior as N V discussed above; Walborn & Panek 1984). Once O stars evolve into supergiants, their winds become dense enough such that Si IV is at the peak of the ionization structure and Si IV is observed in P-Cygni (Drew 1989; Pauldrach et al. 1990). Since the BPASS models incorporate more evolved stars than the STARBURST99 models, BPASS models have strong Si IV and He II features, while STARBURST99 models do not (Fig. 1). Similarly, He II emission comes from evolved stars which are likely in binary pairs (Eldridge et al. 2017). We do observe He II emission in a small subset of the sample, and we discuss both the Si IV and He II features in more detail in Section 6.1.2.

C IV is strong, and in P-Cygni, for all of the MEGaSaURA galaxies. This is largely because C IV probes gas within the winds of 1-10 Myr old stars (Fig. 1). This means that C IV ideally studies the stellar wind profiles and their dependence on stellar age and metallicity. Unfortunately, most of the COS data do not have wavelength coverage of this crucial age and metallicity diagnostic, but it falls in the peak sensitivity of the MEGaSaURA data. In the next two sub-sections, we use the predicted and observed C IV line profiles from the MEGaSaURA sample to explore the stellar properties and how the fitted ages and metallicities in Section 3.4 relate to the morphology of the C IV stellar wind profile.

5.1.2 *Ages from stellar wind lines*

Stellar winds from massive stars are radiation driven (Lamers & Cassinelli 1999), thus both the terminal velocity and mass-outflow rates sensitively depend on the brightness of the star (Lamers & Leitherer 1993; Lamers et al. 1995; Leitherer et al. 1995). The terminal velocity describes the maximal velocity extent of the absorption component, while the mass-loss determines the amount of gas in the outflow and, therefore, the depth and height of the P-Cygni absorption and emission. Since the stellar luminosity strongly depends on age, the stellar population age sensitively sets the shape of the stellar wind P-Cygni profiles of stellar winds (maximum extent, depth of the absorption, and height of the emission components).

The sensitivity of the P-Cygni profile on stellar age is shown by the theoretical 0.2 $Z_{\odot}$ single-aged stellar populations (SSP) STARBURST99 C IV line in the top panel of Fig. 2. At very young ages (2 Myr in this case; the blue line) the C IV profile is dominated by redshifted emission and deep blueshifted absorption that extends blueward to -2000 km s^{-1} . As the stellar population ages to 8 Myr, the stars become less luminous, driving slower and less massive stellar winds. The decreased outflow strength is seen in the 8 Myr year old STARBURST99 model (green line) which does not have a strong emission component, but still has moderately blueshifted absorption that does not extend as far to the blue as the 2 Myr model. By 20 Myr, the stellar population is no longer luminous enough to drive stellar winds, and the C IV line profile becomes narrow and nearly photospheric.

This temporal stellar wind evolution is seen in the MEGaSaURA spectra. The dark solid lines in the lower three panels of Fig. 2 are the STARBURST99 SSPs shown in the upper panel, but now overlaid on three MEGaSaURA spectra with the corresponding stellar age (descending age in each panel). Each of the observed stellar populations have nearly the same fitted metallicities (0.29 ± 0.06 $Z_{\odot}$) to avoid influences from the metallicity of the stars. The strong C IV emission and deep absorption of the 2 Myr model nicely matches the RCS 0327 Knot E spectra, indicating that this galaxy has a young stellar population. Meanwhile, Knot G from the same galaxy has little P-Cygni emission (although note the narrow nebular C IV emission) and less extended absorption, similar to the 8 Myr SSP. Finally, the C IV absorption from J1226+2152, is narrow and similar to the 20 Myr STARBURST99 SSP.

The observed C IV wind lines match the large scale features of the individual SSPs, but certain features are different. The C IV absorption from RCS 0327 Knot G is deeper at blue velocities than the 8 Myr SSP, while J1226+2152 has a small amount of redshifted emission. These galaxies are certainly not SSPs, but the SSP corresponding to the light-weighted age largely captures the profiles of the stellar winds. The multi-age continua fits (BPASS fits in dashed lines and STARBURST99 fits in dot-dashed lines) reproduce many of the observed wind features that the SSP does not by combining wind profiles from multiple epochs (bursts) of star formation. The derived light-weighted ages nicely agree with the correspondence between the SSPs seen by eye: Knot E, Knot G, and J1226+2152 have STARBURST99 light-weighted ages of 2.5, 9.6, and 26 Myr, respectively. The stellar wind morphology diagnoses the stellar population age.

5.1.3 Metallicities from stellar wind lines

Metals in the atmospheres of hot stars absorb continuum photons. This absorbed momentum accelerates the gas off the surface and into a stellar wind. Consequently, the stellar metallicity determines both the acceleration and mass outflow rate of the stellar wind (Lamers & Cassinelli 1999). The terminal velocity (maximal velocity extents of the P-Cygni features) and mass-loss rates (depths of the P-Cygni features) of O-stars has been empirically determined to scale with the stellar metallicity as $Z_s^{0.13}$ and $Z_s^{0.69}$, respectively (Leitherer et al. 1992; Vink et al. 2001). This means that the stellar metallicity sensitively shapes of the P-Cygni features.

In the models, metallicity strongly impacts the C IV line profile (top panel of Fig. 3). we plot the STARBURST99 synthetic C IV wind profile for three metallicities (0.2, 0.4, and 1.0 $Z_\odot$), with the same 4 Myr age. The C IV emission of the 0.4 and 1.0 $Z_\odot$ cases have similar heights and widths, but the 0.2 $Z_\odot$ case has 20% less emission. Further, the 1.0 $Z_\odot$ absorption component is deeper (has a larger mass-loss rate) and extends further to the blue (has a larger maximal velocity) than the low metallicity cases. The stellar wind morphologies are sensitive metallicity diagnostics.

The observed stellar wind profiles similarly vary with the light-weighted metallicity of the galaxies. The lower three panels show three galaxies with light-weighted metallicities of 0.31, 0.71, and 1.0 $Z_\odot$, but all with ages of 4 ± 1 Myr. RCS 0327 Knot U

5.2 Photospheric lines

6 DISCUSSION

6.1 Comparing BPASS and STARBURST99 models

6.1.1 Similar ages and metallicities

6.1.2 The He II 1640 Å region

J0108+0624 has a He II equivalent width of -0.30 Å with a width of 96 km s^{-1}. The Planck Arc has an equivalent width of -1.19Å and a velocity width of 379 km s^{-1} . The emission lines peak slightly blueward of zero-velocity (-65 and -29 km s^{-1}). Crowther et al. (2010) also observed large He II equivalent widths from the young stellar population in the Tarantula Nebula. The authors suggest that the large equivalent widths are due to clumpy, rapidly rotating stars.

6.2 The similarity between stellar and gas-phase metallicities

6.3 The ionizing continua of massive stars

6.4 Continuous versus instantaneous star formation

In Section 5.1.2 we emphasized how our high signal-to-noise and moderate spectral resolution UV observations diagnose the stellar population age using O and B-star features. In Fig. 2, we showed that the stellar wind lines are sensitive to the age of the stellar population. Young populations show deep and wide C IV P-Cygni features, while older stellar populations have more moderate features. Similarly, the populations younger than 4 Myr have O V 1371Å wind features, while these features are absent in older populations. The stellar wind lines diagnose young stars and the photospheric lines diagnose older stellar populations. The youngest stellar populations do not show the 1290Å photospheric lines, while the oldest stellar populations show strong photospheric lines (Fig. 4). The observed UV stellar continua are discrete bursts of star formation stellar bursts, and not the product of continuous star formation.

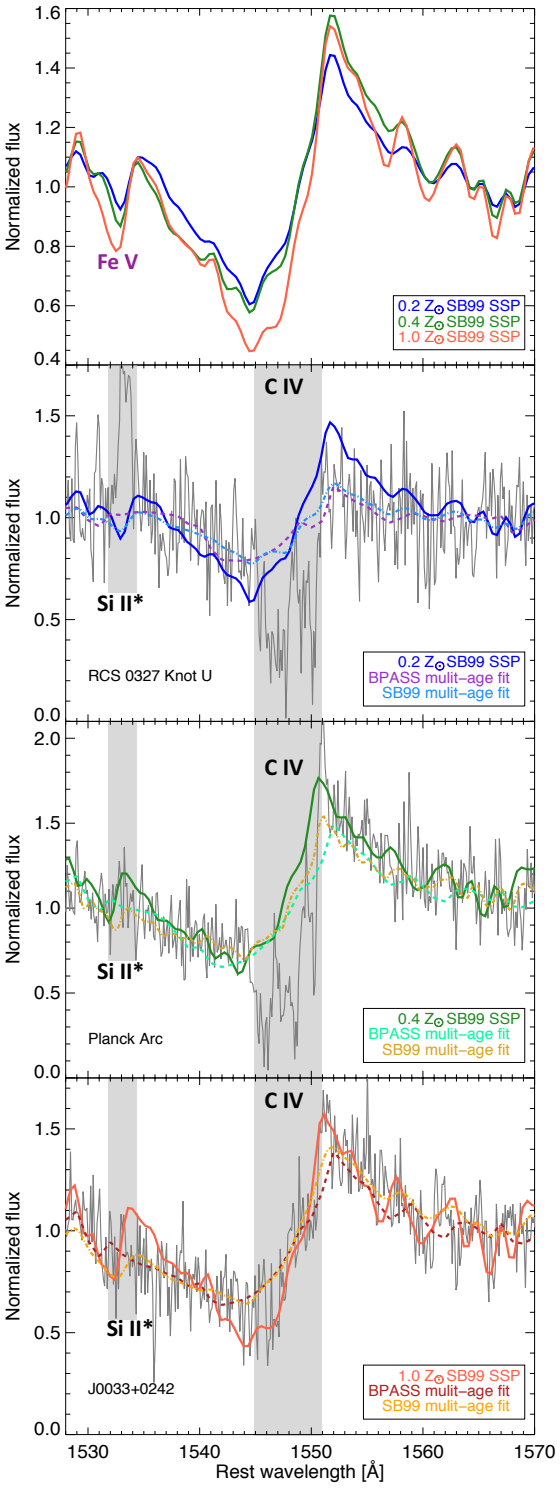

Figure 3. Similar to Fig. 2 but for the variation of the C IV O-star wind region with stellar metallicity. The top panel shows three different STARBURST99 single stellar populations (SSP) with metallicities of 0.2, 0.4, and 1.0 $Z_\odot$ and the same 4 Myr age. The C IV profile absorption is deeper and the emission is stronger with increasing metallicity. The next three panels show three galaxies (names in the lower left) with descending fitted metallicities of 0.31, 0.71, and 1.0 $Z_\odot$ and fitted ages of 4 ± 1 Myr. The SSP that corresponds to the fitted properties are over-plotted as a solid lines. The multi-age, multi-metallicity BPASS (dashed line) and STARBURST99 (dot-dashed line) are shown in each panel. Gray regions indicate interstellar C IV absorption and Si II* emission.

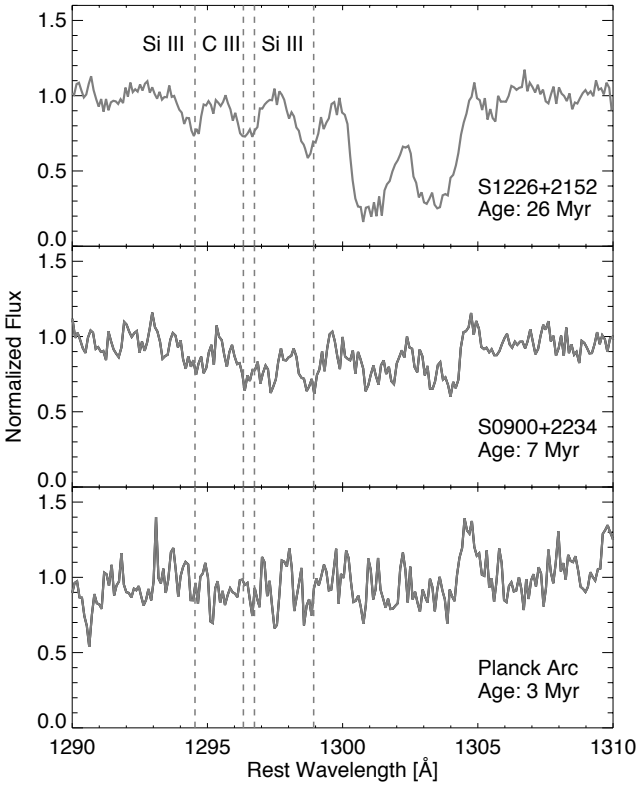

Figure 4. The photospheric absorption region (1290–1300Å) for three galaxies: S1226+2152 (top panel), S0900+2234 (middle panel), and the Planck Arc (bottom panel). The four photospheric absorption lines (see Table 1) are marked by dashed gray lines and their transitions are labelled in the top panel. These lines originate in the photospheres of B-type stars with ages greater than 8 Myr. The photospheric lines strengthen with increasing fitted age, indicating that the fitted ages reflect the transition from O-star dominated spectra to B-star dominated spectra.

The instantaneous burst observation has important consequences for the determination of the number of ionizing photons. By constantly forming stars at the same rate for 100 Myr, the SED is a time average of the stars over 100 Myr. This causes a 100 Myr continuous star-formation history (commonly used in the literature to determine the ionizing continua; Steidel et al. 2016, 2018) to have a substantially lower ionizing continua than instantaneous bursts of similar metallicity (compare the red dot-dashed line to the other dot-dashed lines in Fig. 8). The reason for this is because the instantaneous burst models can have significant contributions from populations like young O-stars (such as a 3 Myr population) or evolved stripped stars (such as a 10 Myr population) that produce hard ionizing spectra, while the continuous star formation case always has to have an average of non-ionizing old stars as well as ionizing young stars. This dilutes the ionizing spectrum.

The SED of a 100 Myr continuously star forming galaxy *under*-produces the number of ionizing photons that are produced by a typical instantaneous burst law (Fig. 8). To produce the observed nebular emission lines, Steidel et al. (2016) found that a metal deficient stellar population with a Z_s 4–5 lower than the ISM metallicities is required to produce sufficiently hard radiation fields to match the observed nebular emission lines. The lower continuously star forming Z_s stellar population produces twice as many 500 Å photons as a higher metallicity model that matches the ISM metallicity, 0.4 $Z_\odot$ (compare the red dashed lines in Fig. 11 and Fig. 8). This produces a sufficiently hard ionizing spectra to replicate the nebular emission lines.

Alternatively, the STARBURST99 (BPASS) instantaneous burst model has a light-weighted metallicity of 0.33 $Z_\odot$ (0.39 $Z_\odot$). The light-weighted Z_s matches the ISM metallicity range of 0.29–0.49 $Z_\odot$ found by Steidel et al. (2016), while the instantaneous BPASS ionizing continua is similar to the continuous SED model used by Steidel et al. (2016). Thus, a linear combination of instantaneous, single-aged stellar populations with an average metallicity equal to the ISM is sufficient to reproduce the observed nebular emission structure without requiring metal deficient stars. Consequently, the instantaneous model suggests that the young stars and the gas surrounding the young stars have a similar metallicities.

This demonstrates that an instantaneous star formation history is possibly a way to reconcile the observed nebular ionization structure and stellar continua, but the relative increased production of ionizing photons from the instantaneous star formation law has important consequences. For instance, star formation rate indicators are typical calibrated assuming constant star formation (Kennicutt 1998), and variations in stellar age will have large impact. Imagine two galaxies with the same UV luminosity but one is dominated by an older stellar population of 15 Myr and the other is dominated by a younger stellar population of 3 Myr. To achieve the same UV luminosity, the older stellar population had to form significantly more stars 15 Myr ago than the younger population did 3 Myr, but if the SFRs are estimated using the UV continua they would be identical. Conversely, SFRs estimated using Hα would indicate that the younger galaxy formed significantly more stars even though it formed significantly fewer stars over the entire burst duration because only stars less than 10 Myr produce appreciable ionizing photons (Kennicutt 1998). Similar effects are imprinted on the dust SED (e.g. the dust temperature), and in turn the IR-based SFRs, because UV-bright, young stellar populations will heat the dust to higher temperatures (Helou 1986).

The SFR situation is more uncertain when different stellar models (STARBURST99 versus BPASS) and different stellar metallicities are considered. As demonstrated in Section 6.3, the number of ionizing photons, and therefore the Hα flux, will drastically depend on the presence of binary stars (Eldridge et al. 2017). A stellar population with a large binary population would produce a larger Hα flux at the same UV luminosity as a single star population. The binary effect is similar, and enhanced, by the hardening of the ionizing spectra at lower metallicities, which may further increase the SFR derived from Hα relative to single star and higher metallicity stellar populations. The uncertainty of the ionizing continua may introduce a large uncertainty to the measured SFRs of galaxies.

How physical is the instantaneous burst assumption? Often times the continuous star formation case is argued when observations average large physical regions within galaxies (Leitherer et al. 1999; Rix et al. 2004), but the light from the highly spatially magnified gravitationally lensed MEGaSaURA galaxies and within the spatially-resolved 2.″5 diameter COS aperture is dominated by individual star-forming regions. This is nicely illustrated by the comparison of the three star-forming knots in RCS 0327 which have similar Z_s, but light-weighted ages of 2.5, 4.7, and 9.6 Myr. The C IV lines profiles dramatically change between the three knots (see Fig. 2 and Fig. 3), indicating that the stellar populations of these three knots have markedly different ages. Even in local galax-

ies, individual UV-bright star-forming knots are bursty and cannot sustain their local SFRs, suggesting that the instantaneous burst model is appropriate for lensed high-redshift galaxies and spatially resolved local observations.

Initially, the young ages measured here and the instantaneous burst star formation histories appear at odds with the 100 Myr ages determined from SED fits of these galaxies (Wuyts et al. 2012). However, it is important to stress here that the quoted ages are light-weighted ages at 1270Å. At this blue wavelength, stars older than 20 Myr are orders of magnitude fainter in the UV and do not significantly contribute to the 1270Å light. Meanwhile, SED fits typically use restframe optical wavelengths between 0.3–1μm, but can extend into the near-IR. At these wavelengths older stellar populations contribute comparable light, consequently the light-weighted ages at optical and near-IR wavelengths will be substantially older than those measured at UV wavelengths.

Stacking should create a stellar population that approaches continuous star formation, however find that the STARBURST99 (BPASS) fitted age and metallicity of 12.7 Myr and 0.45 Z$-\odot$ (8.6 Myr and 0.65 Z$_\odot$) for the MEGaSaURA stack is consistent with the signal-to-noise at 1600 Å weighted average of the MEGaSaURA sample of 13.5 Myr and 0.50 Z$_\odot$ (8.5 Myr and 0.63 Z$_\odot$). Consequently, stacked spectra are simply the light-weighted average of the different stellar populations in the stack, many of which have similar, moderate age and Z$_s$, stellar populations. This suggests that the instantaneous burst scenario may be appropriate for stacks comprising moderate numbers of galaxies or with similar stellar populations. Different star formation histories can have dramatic effects on the ionizing continua and care is required when determining the ionizing continua of galaxies.

This paper has been typeset from a TEX/LATEX file prepared by the author.

REFERENCES

Asplund M., Grevesse N., Sauval A. J., Scott P., 2009, ARA&A, 47, 481
Calzetti D., Armus L., Bohlin R. C., Kinney A. L., Koornneef J., Storchi-Bergmann T., 2000, ApJ, 533, 682
Chisholm J., Tremonti C. A., Leitherer C., Chen Y., Wofford A., Lundgren B., 2015, ApJ, 811, 149
Chisholm J., Tremonti C. A., Leitherer C., Chen Y., Wofford A., 2016, MNRAS, 457, 3133
Crowther P. A., Schnurr O., Hirschi R., Yusof N., Parker R. J., Goodwin S. P., Kassim H. A., 2010, MNRAS, 408, 731
Drew J. E., 1989, ApJS, 71, 267
Eldridge J. J., Stanway E. R., Xiao L., McClelland L. A. S., Taylor G., Ng M., Greis S. M. L., Bray J. C., 2017, Publ. Astron. Soc. Australia, 34, e058
Green J. C., et al., 2012, ApJ, 744, 60
Helou G., 1986, ApJ, 311, L33
Jones T., Stark D. P., Ellis R. S., 2012, ApJ, 751, 51
Kennicutt Jr. R. C., 1998, ApJ, 498, 541
Kroupa P., 2001, MNRAS, 322, 231
Kudritzki R. P., 1998, in Aparicio A., Herrero A., Sánchez F., eds, Stellar astrophysics for the local group: VIII Canary Islands Winter School of Astrophysics. p. 149
Lamers H. J. G. L. M., Cassinelli J. P., 1999, Introduction to Stellar Winds. Cambridge, UK: Cambridge University Press
Lamers H. J. G. L. M., Leitherer C., 1993, ApJ, 412, 771
Lamers H. J. G. L. M., Snow T. P., Lindholm D. M., 1995, Terminal Velocities and the Bistability of Stellar Winds, doi:10.1086/176575
Le Borgne J.-F., et al., 2003, A&A, 402, 433
Leitherer C., Robert C., Drissen L., 1992, ApJ, 401, 596
Leitherer C., Chapman J. M., Koribalski B., 1995, ApJ, 450, 289
Leitherer C., et al., 1999, ApJS, 123, 3
Leitherer C., Ortiz Otálvaro P. A., Bresolin F., Kudritzki R.-P., Lo Faro B., Pauldrach A. W. A., Pettini M., Rix S. A., 2010, ApJS, 189, 309
Leitherer C., Ekström S., Meynet G., Schaerer D., Agienko K. B., Levesque E. M., 2014, ApJS, 212, 14
Markwardt C. B., 2009, in Bohlender D. A., Durand D., Dowler P., eds, Astronomical Society of the Pacific Conference Series Vol. 411, Astronomical Data Analysis Software and Systems XVIII. p. 251 (arXiv:0902.2850)
Marshall J. L., et al., 2008, in Ground-based and Airborne Instrumentation for Astronomy II. p. 701454 (arXiv:0807.3774), doi:10.1117/12.789972
Meynet G., Maeder A., Schaller G., Schaerer D., Charbonnel C., 1994, A&AS, 103, 97
Pauldrach A. W. A., Kudritzki R. P., Puls J., Butler K., 1990, A&A, 228, 125
Rigby J. R., et al., 2018a, AJ, 155, 104
Rigby J. R., et al., 2018b, ApJ, 853, 87
Rivera-Thorsen T. E., Östlin G., Hayes M., Puschnig J., 2017, ApJ, 837, 29
Rix S. A., Pettini M., Leitherer C., Bresolin F., Kudritzki R.-P., Steidel C. C., 2004, ApJ, 615, 98
Shapley A. E., Steidel C. C., Pettini M., Adelberger K. L., 2003, ApJ, 588, 65
Stanway E. R., Eldridge J. J., Becker G. D., 2016, MNRAS, 456, 485
Steidel C. C., Strom A. L., Pettini M., Rudie G. C., Reddy N. A., Trainor R. F., 2016, ApJ, 826, 159
Steidel C. C., Bogosavlevic M., Shapley A. E., Reddy N. A., Rudie G. C., Pettini M., Trainor R. F., Strom A. L., 2018, preprint, (arXiv:1805.06071)
Vink J. S., de Koter A., Lamers H. J. G. L. M., 2001, A&A, 369, 574
Wakker B. P., Hernandez A. K., French D. M., Kim T.-S., Oppenheimer B. D., Savage B. D., 2015, ApJ, 814, 40
Walborn N. R., Panek R. J., 1984, ApJ, 280, L27
Westera P., Lejeune T., Buser R., Cuisinier F., Bruzual G., 2002, A&A, 381, 524
Wuyts E., Rigby J. R., Sharon K., Gladders M. D., 2012, ApJ, 755, 73
de Mello D. F., Leitherer C., Heckman T. M., 2000, ApJ, 530, 251

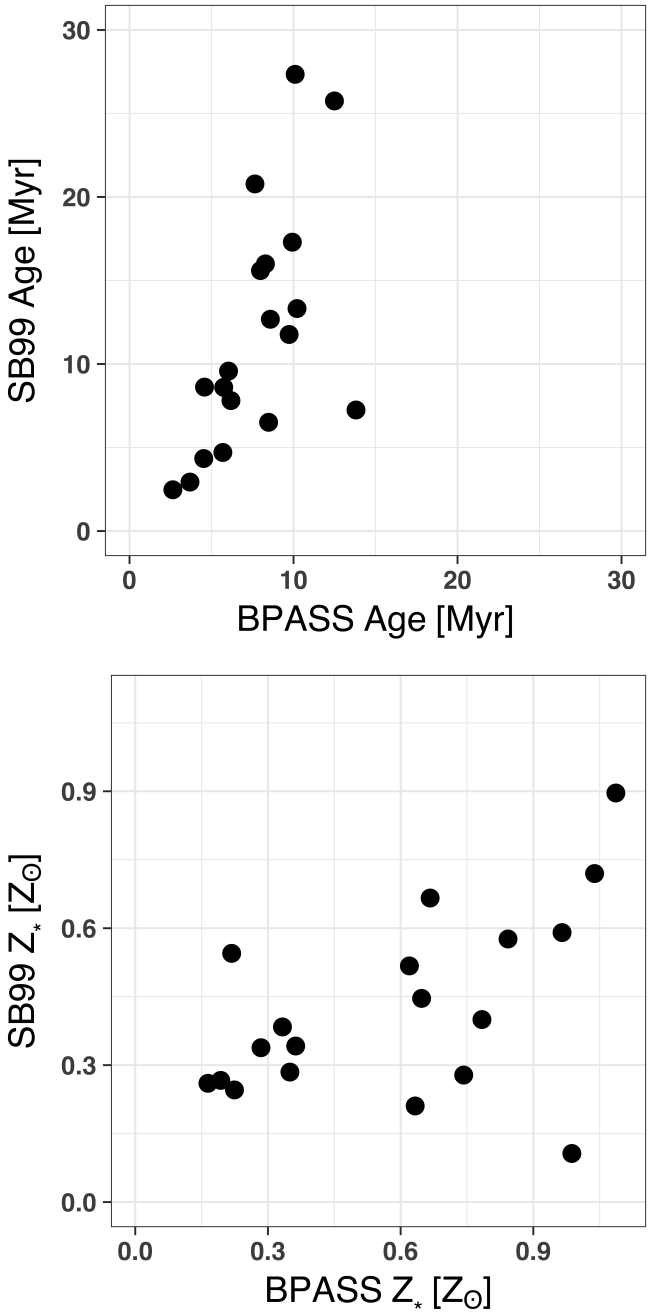

Figure 5. *Top Panel:* Comparison of the light-weighted stellar ages computed using STARBURST99 (SB99) and BPASS stellar templates. The BPASS ages do not extend past 10 Myr largely because high-resolution stellar templates do not exist for these ages. Consequently, the oldest BPASS ages are 10-15 Myr. There is a general trend where galaxies designated as old with BPASS are designated as old with STARBURST99. *Bottom Panel:* Comparison of the light-weighted stellar metallicities (Z_s) computed using STARBURST99 and BPASS stellar templates.

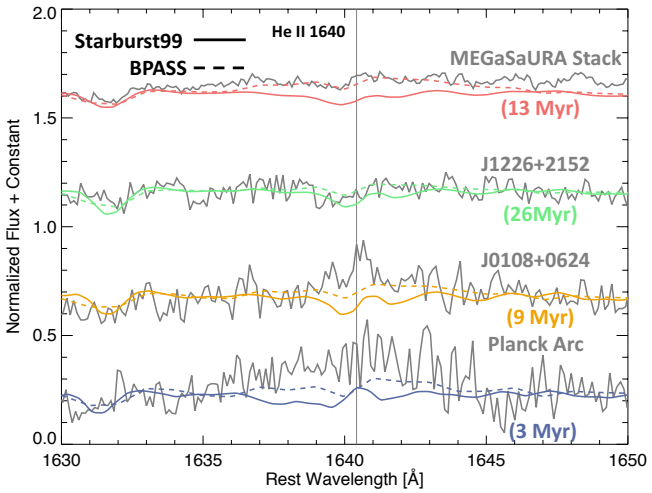

Figure 6. The He II spectral region for four spectra: the MEGaSaURA stack (top spectra), J1226+2152 (top middle spectra), J0108+0624 (bottom middle spectra), and the Planck Arc. Overplotted on each is the STARBURST99 (solid line) and BPASS multi-age stellar population fit of each spectrum. Generally, the BPASS models fit the He II region far better than the STARBURST99 models, especially for the high signal-to-noise MEGaSaURA stack. Conversely, nether model adequately fit J0108+0624 nor the Planck Arc (bottom two spectra). J0108+0624 has narrow emission (96 km s^{-1}) that is likely nebular in origin, while the Planck Arc has broad emission (379 km s^{-1}) that is likely stellar in origin. RCS 0327 knot E (another very young stellar population) has similarly broad He II emission.

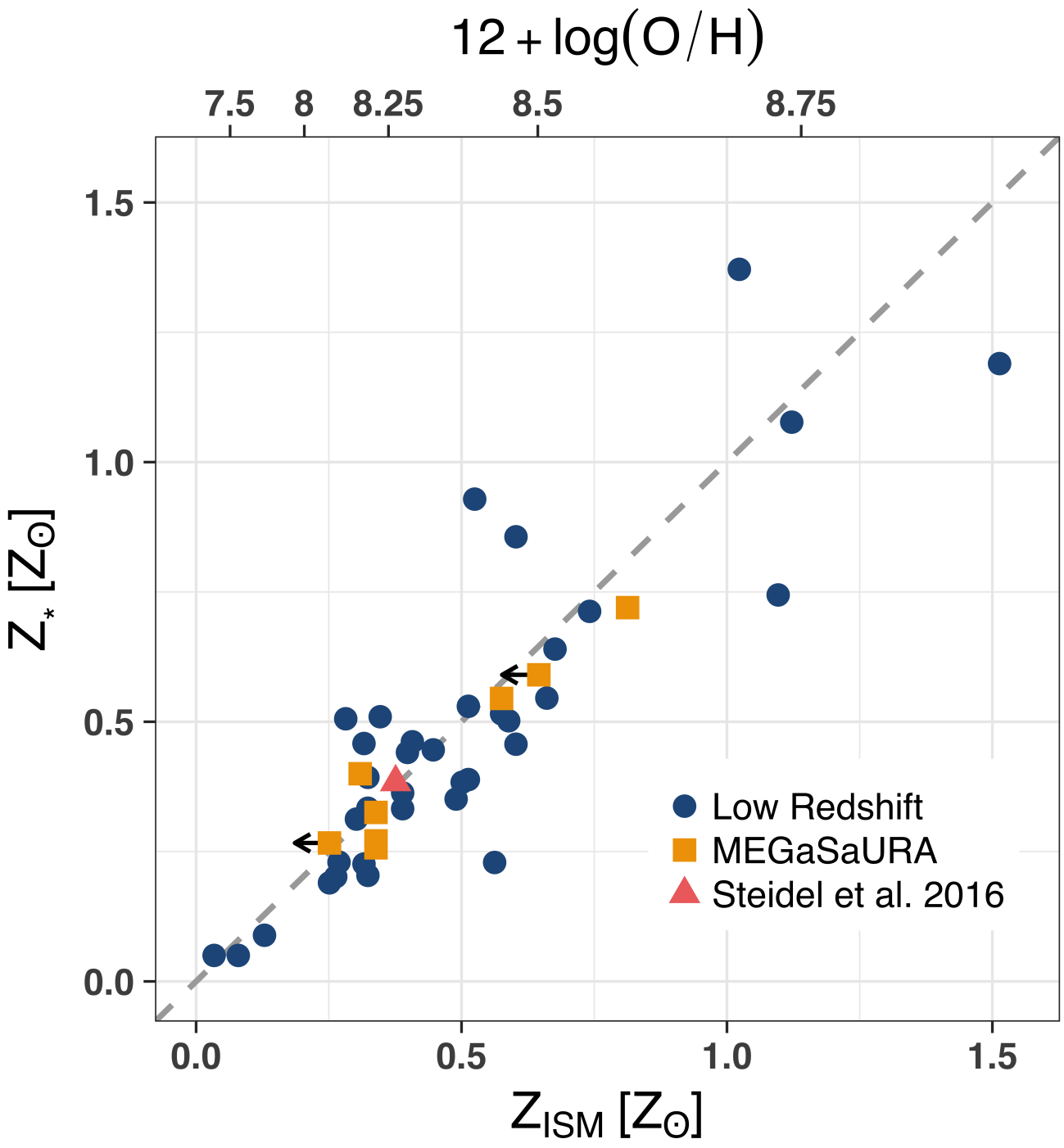

Figure 7. Comparison of the light-weighted stellar metallicity (Z_s) derived from the STARBURST99 fitting to the gas-phase ISM metallicity (Z_{ISM}). The points are color-coded from the three samples: blue circles are low-redshift galaxies, orange squares are the individual $z \sim 2$ galaxies from the MEGaSaURA sample, and the red triangle is the stacked sample from Steidel et al. (2016). A one-to-one line is shown in gray: Z_s is largely equivalent to Z_{ISM}.

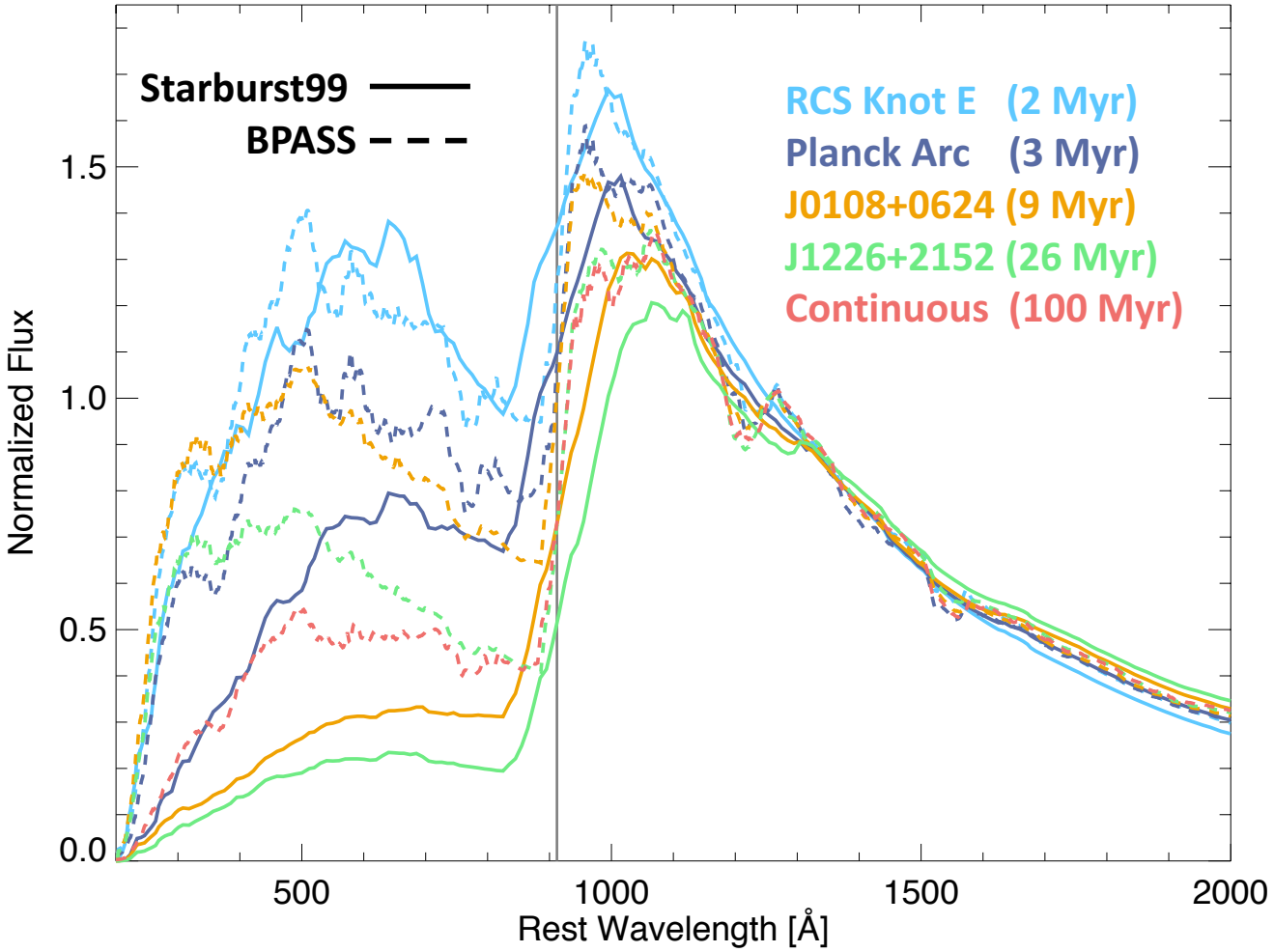

Figure 8. The fitted, theoretical spectral energy distributions (SEDs), normalized at 1270Å, for four galaxies: RCS 0327 knot E (light blue), the Planck Arc (dark blue), J0108+0624 (orange), and J1226+2152 (green). We plot both the best-fit STARBURST99 (solid line) and BPASS models (dashed line). All models are significantly smoothed to high-light the overall shape of the ionizing continua (blueward of 912Å as marked by the vertical gray line). For both models, the ionizing continua increases with fitted stellar population age (ages are given on the right), such that younger populations produce more ionizing photons. The BPASS models of older stellar populations produce significantly more ionizing photons than the STARBURST99 models due to the effects of binaries. The BPASS models suggest that J0108+0624 produces similar relative amounts of He II ionizing photons (blueward of 227Å) as the much younger stellar population of RCS 0327 Knot E. This may explain the observed He II nebular emission from J0108+0624 in Fig. 6. A 0.4 $Z_{\odot}$ BPASS model with continuous star-formation over 100 Myr is included in red and has a relatively lower ionizing continua than the J1226+2152 fit.

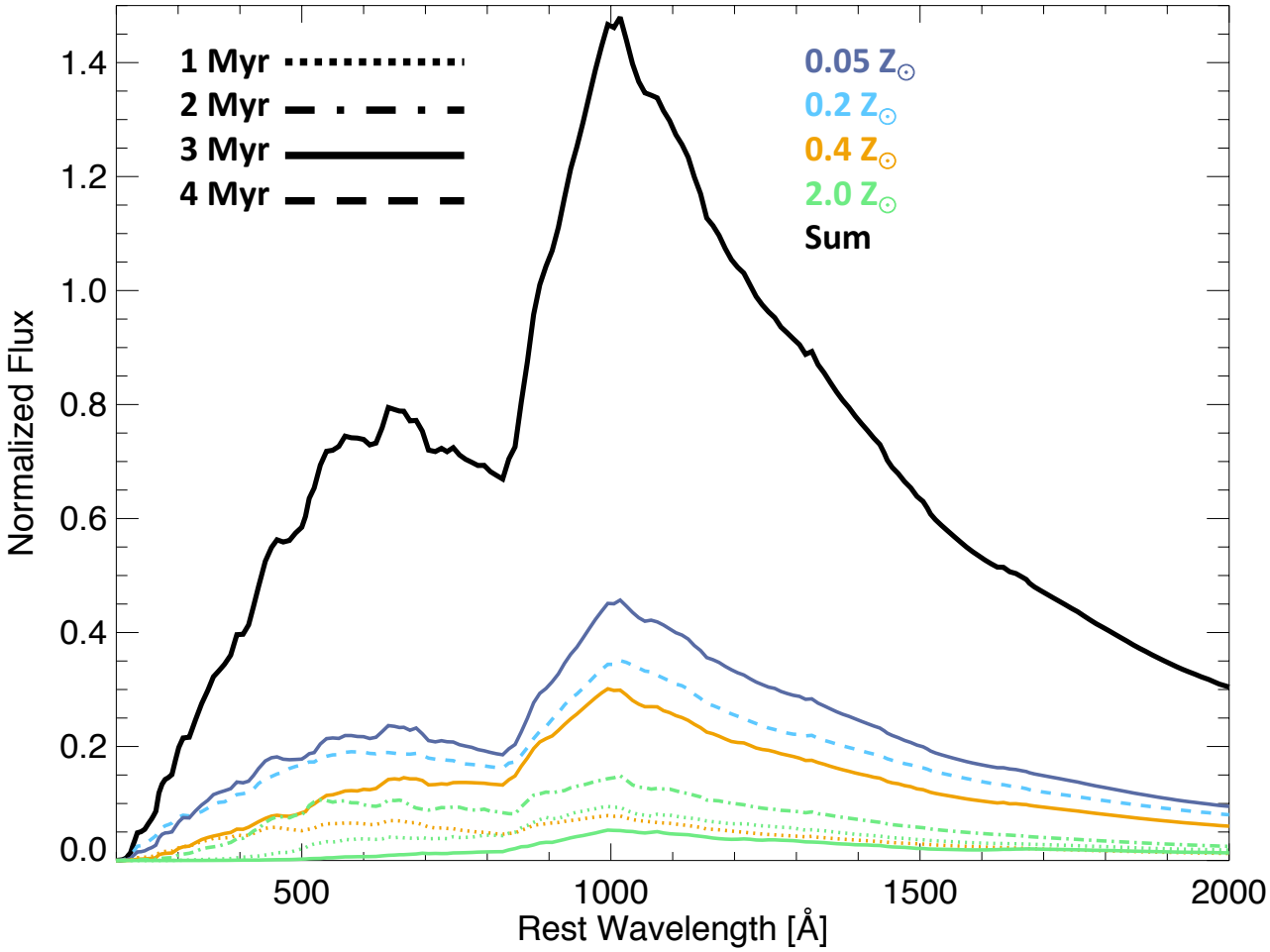

Figure 9. The fitted STARBURST99 ionizing continuum for the Planck Arc (black). Overplotted are the individual stellar models that comprise the total sum. Each stellar metallicity is color-coded and the line types mark the ages of the stellar population. The ionizing continuum is mostly determined by a 0.05 $Z_\odot$ 3 Myr and 0.2 $Z_\odot$ 2 Myr model.

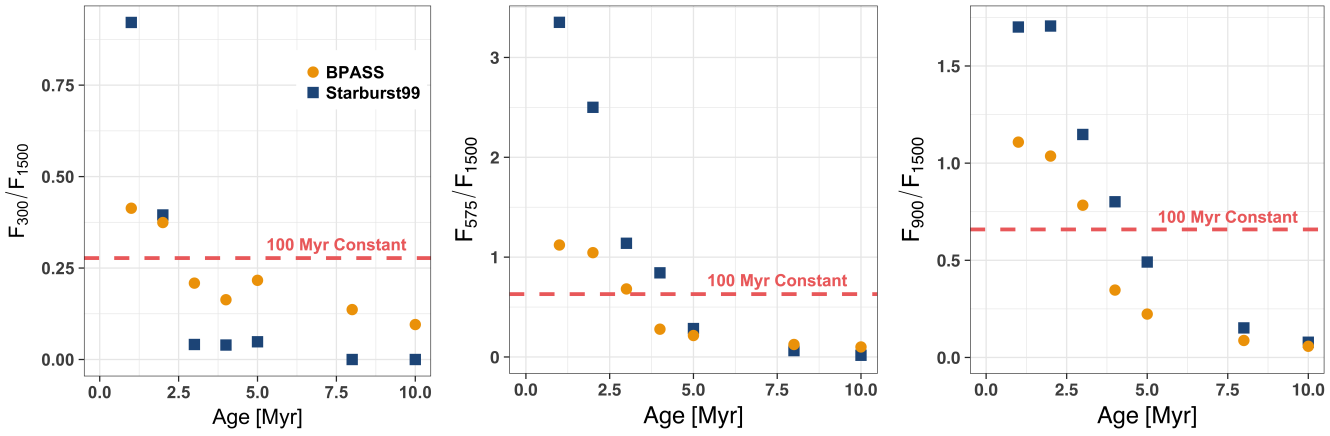

Figure 10. The temporal variation (in Myr) of the ratio of the ionizing-to-nonionizing flux at three wavelengths of ionizing flux (300, 575, and 900Å from left to right) of theoretical 0.4 $Z_{\odot}$ single stellar populations. We include flux ratios corresponding to both STARBURST99 (blue squares) and BPASS models (gold circles). STARBURST99 populations have larger ionizing flux at redder wavelengths (575 and 900Å) and younger ages, but the ionizing flux of evolved BPASS models surpasses STARBURST99 models at bluer wavelengths (higher energies). We include the flux ratios of a BPASS model with constant star formation as a dashed red line in all panels. The constant star formation model has similar properties as a 3 Myr stellar population.

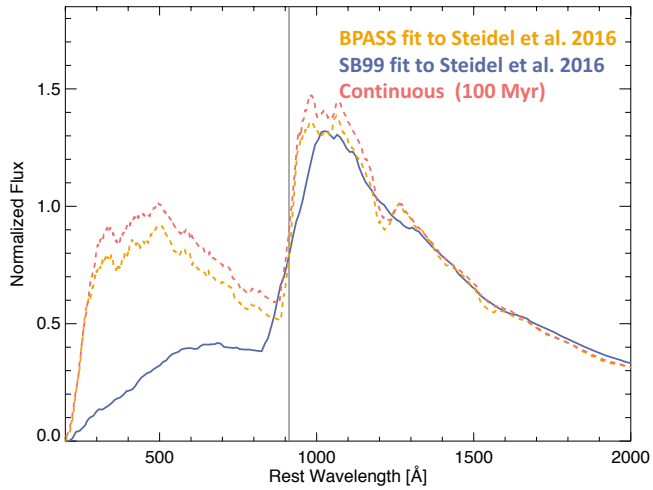

Figure 11. Comparison of the best-fit multi-age instantaneous burst histories using BPASS (in orange with a light-weighted age of 10 Myr and 0.33 $Z_{\odot}$, respectively) and STARBURST99 (blue with a light-weighted age and metallicity of 12 Myr and 0.39 $Z_{\odot}$, respectively) models to the 0.05 $Z_{\odot}$ constant star formation history model used by Steidel et al. (2016) (red). Models using BPASS are plotted as dashed lines and STARBURST99 models are solid. Notice the similarity between the constant and instantaneous BPASS models, even though the instantaneous burst is significantly more metal enriched, and similar to the ISM metallicity of 0.29–0.49 $Z_{\odot}$ found by Steidel et al. (2016), than the continuous star formation model. By using an instantaneous burst history the gas and stars have similar metallicities which eliminates the need for stars to have significantly lower metallicities than the gas (Steidel et al. 2016).